Supporting Information

Anion influence on synthesis of Cu(I)-based coordination polymers along with a series of derived materials for the selective photocatalysis properties

Xiao-Sa Zhang,[a] Jia-Liang Cui,[a] Yu Liu,[a] Wen-Ze Li,[*a] Yan Liu,[a] Hong Xiang,[a] Jian Luan[*b]

[a] College of Science, Shenyang University of Chemical Technology, Shenyang, 110142, P. R. China

[b] College of Sciences, Northeastern University, Shenyang, 110819, P. R. China

E-mails: liwenze@syuct.edu.cn; 2010044@stu.neu.edu.cn

Table S1 Selected bond distances (Å) and angles (°) for CP **1**.

Cu(1)–N(1)	2.031(2)	Cu(1)–Cl(1)	2.3836(8)
Cu(1)–N(2)	2.046(2)	Cu(1)–Cl(1)#1	2.4240(8)
N(1)–Cu(1)–N(2)	112.68(8)	N(1)–Cu(1)–Cl(1)#1	106.17(7)
N(1)–Cu(1)–Cl(1)	117.17(7)	N(2)–Cu(1)–Cl(1)#1	110.97(7)
N(2)–Cu(1)–Cl(1)	105.96(6)	Cl(1)–Cu(1)–Cl(1)#1	103.52(3)

Symmetry code: #1 –x, –y, –z.

Table S2 Selected bond distances (Å) and angles (°) for CP **2**.

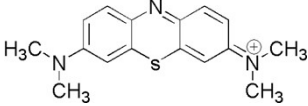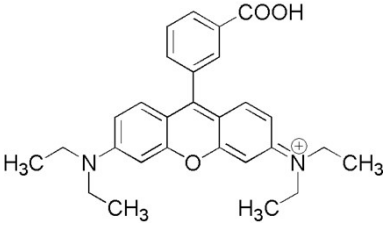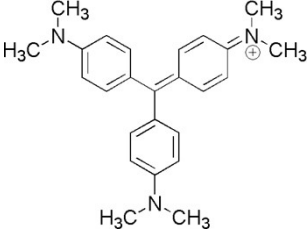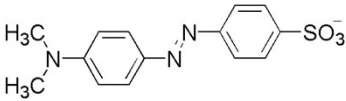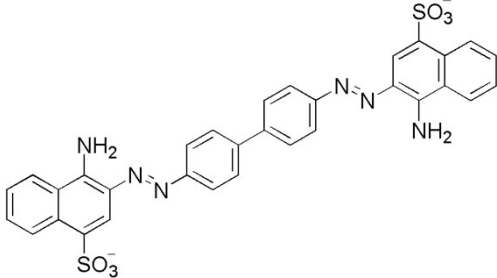|			
Cu(1)–N(1)	1.9239(17)	Cu(1)–O(1)#1	2.438(2)
Cu(1)–N(1)#1	1.9239(17)	Cu(1)–O(1)	2.438(2)
N(1)–Cu(1)–N(1)#1	156.16(10)	N(1)–Cu(1)–O(1)	96.28(8)
N(1)–Cu(1)–O(1)#1	105.29(8)	N(1)#1–Cu(1)–O(1)	105.29(8)
N(1)#1–Cu(1)–O(1)#1	96.28(8)	O(1)#1–Cu(1)–O(1)	50.70(10)

Symmetry code: #1 –x – 1/2, –y + 2, z.

Supporting Information

Table S3 Hydrogen bonding geometries (Å, °) of CPs **1** and **2**.

CP	D–H···A	D–H	H···A	D···A	D–H···A
1	C3–H3A···O2[a]	0.93	2.53	3.2468	134
	O1W–H1WA···N4[b]	0.85	2.06	2.9055	171
	O1W–H1WB···Cl1[c]	0.85	2.62	3.4711	178
2	N(2)–H(2B)···O(3)[d]	0.86	2.14	2.9410	155
	C(2)–H(2A)···O(1)[e]	0.93	2.58	3.2573	130

Symmetry codes: [a] $1 - x$, $-y$, $1 - z$; [b] $1 - x$, $1 - y$, $1 - z$; [c] $1 - x$, $-y$, $-z$; [d] x, $1 + y$, z; [e] $1 - x$, $1 + y$, $1/2 - z$.

Table S4 Organic dyes with different charge types and sizes.

Dye	Formula	Charge type	Size (nm × nm × nm)
Methylene Blue (MB)		Cationic	$0.40 \times 0.79 \times 1.63$
Rhodamine B (RhB)		Cationic	$0.68 \times 1.18 \times 1.57$
Gentian Violet (GV)		Cationic	$0.40 \times 1.30 \times 1.37$
Methyl Orange (MO)		Anionic	$0.53 \times 0.73 \times 1.74$
Congo Red (CR)		Anionic	$0.39 \times 0.86 \times 2.61$

Supporting Information

Table S5 Comparison of photodegradation efficiency of different materials for GV.

Material	Dosage (mg)	Irradiation time (min)	Degradation efficiency (%)	Reference
TiO_2 P25	1000	30	100	S1
C-V-1	5	30	99.01	S2
Cu@TiO_2	5	240	99.51	S3
TiO_2/$CoFe_2O_4$	5	180	83.00	S4
Ni-CP@FA-1000	5	240	100	S5
Cu/CuO@C	10	240	93.22	S6
Cu@N-1	5	240	97.79	This work

References:

S1 S. Bendjabeur, R. Zouaghi, O. N. H Kaabeche and T. Sehili, *Int. J. Chem. React. Eng.*, 2017, **15**, 20160206.

S2 X. S. Zhang, H. T. Zhao, Y. Liu, W. Z. Li, A. A. Yang and J. Luan, *Dalton Trans.*, 2021, **50**, 18173–18185.

S3 Y. Q. Zhang, N. Xu, Y. Liu, X. S. Zhang, W. Z. Li, H. T. Zhao and J. Luan, *RSC Adv.*, 2022, **12**, 9363–9372.

S4 I. Ibrahim, G. V. Belessiotis, A. M. Elseman, M. M. Mohamed, Y. Ren, T. M. Salama and M. B. I. Mohamed, *Nanomaterials*, 2022, **12**, 3290.

S5 Y. X. Li, W. L. Duan, J. Luan and F. Guo, *Inorg. Chim. Acta*, 2023, **549**, 121418.

S6 W. L. Duan, X. Liu, J. Luan, G. R. Jiao, Z. Y. Jiang and F. Yan, *J. Solid State Chem.*, 2023, **322**, 123995.
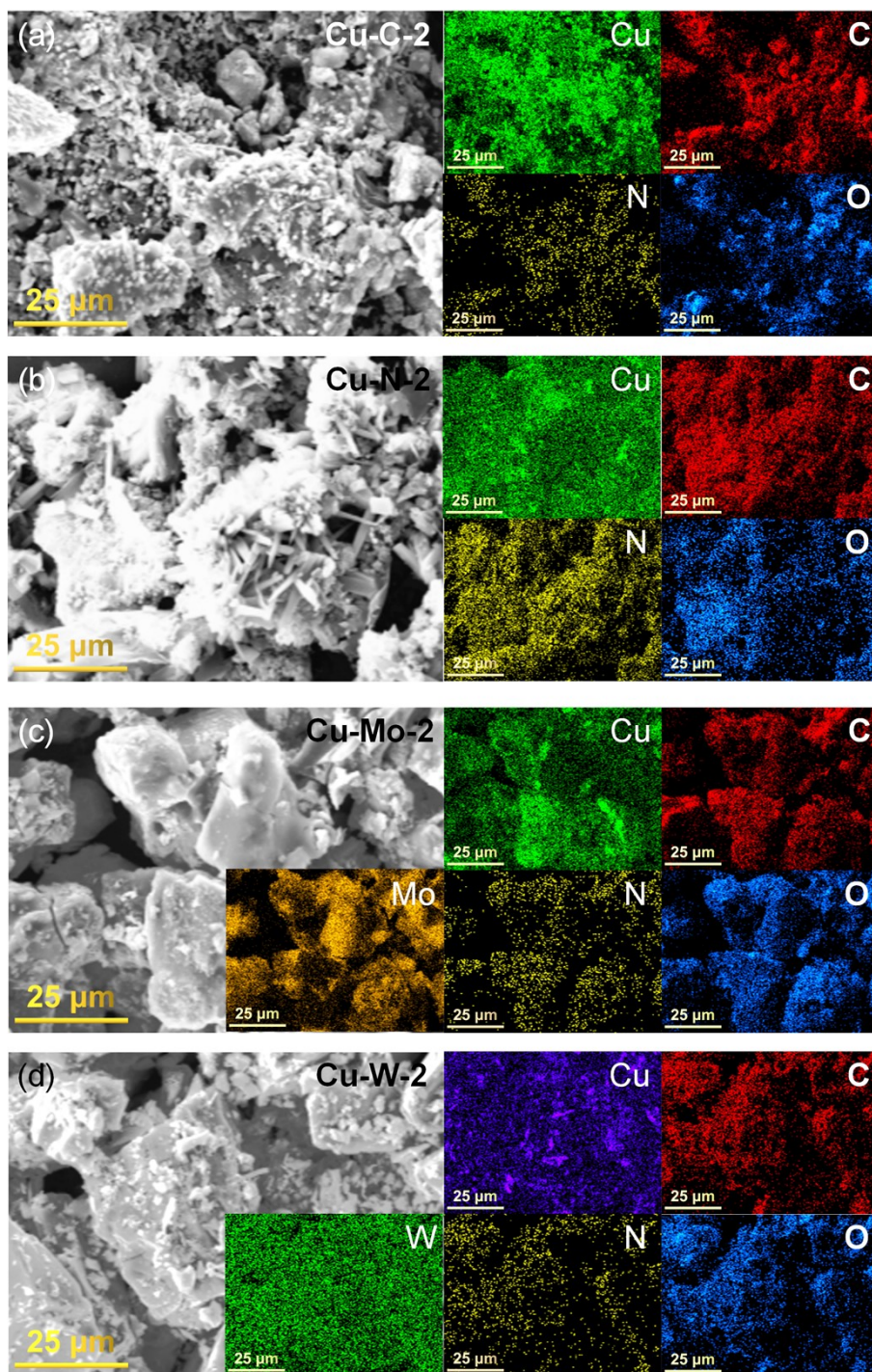
Fig. S1 Typical SEM images and corresponding element mappings of **Cu-C-2** (a), **Cu-N-2** (b), **Cu-Mo-2** (c), **Cu-W-2** (d).
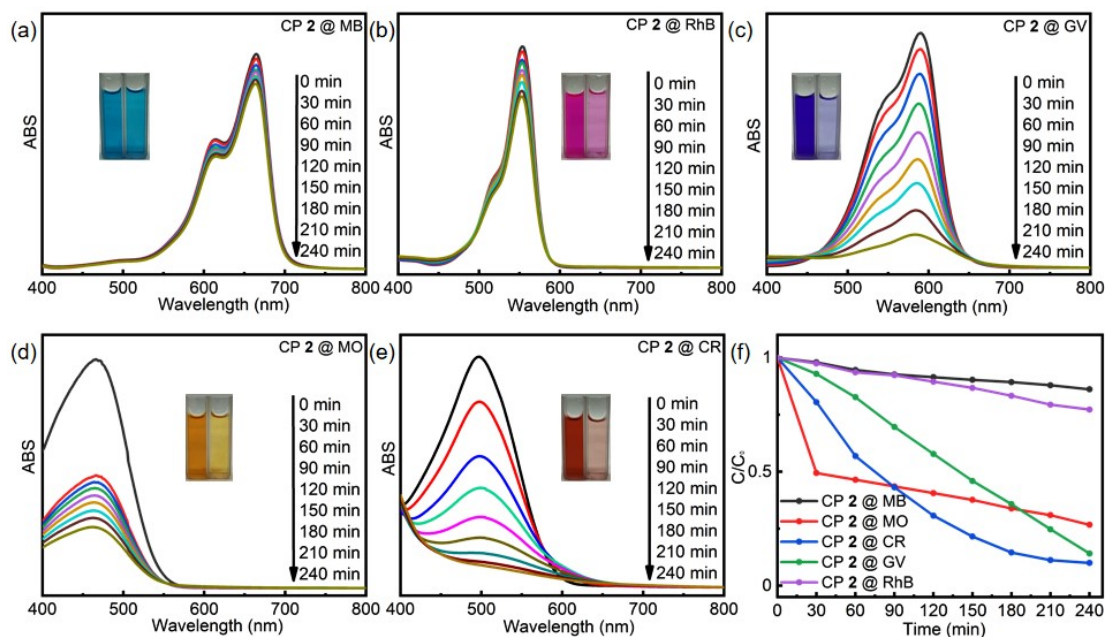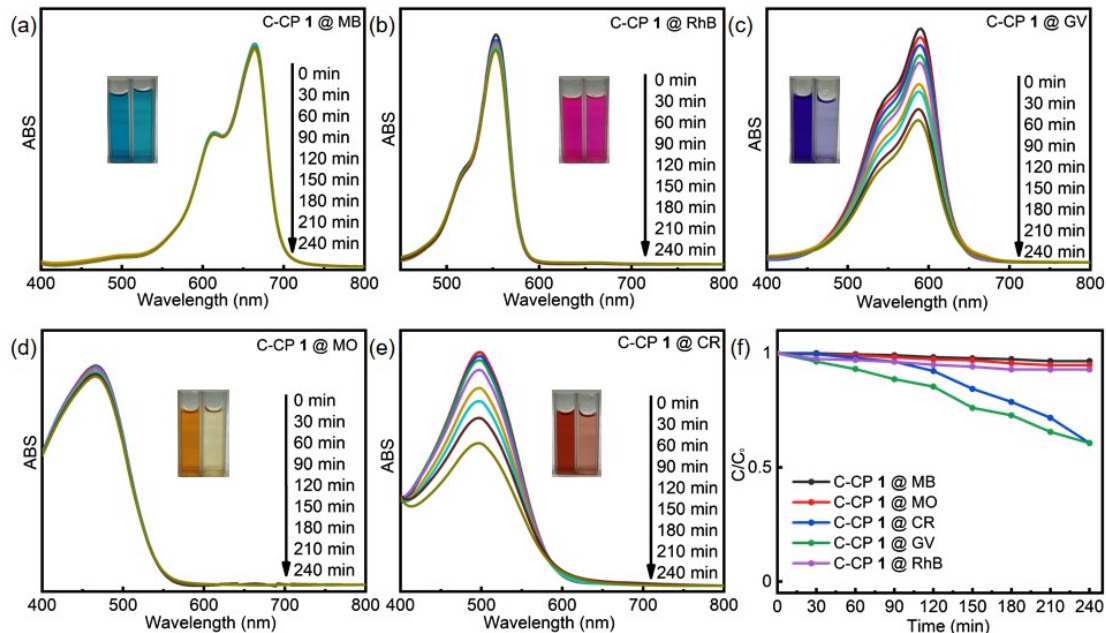
Fig. S2 UV–vis spectra of MB (a), RhB (b), GV (c), MO (d), and CR (e) solutions which were recorded after photocatalytic degradation had been performed for different lengths of time with CP **2**. (f) The photodegradation rates of MB, RhB, MO, CR and GV at different time points during exposure to CP **2**.
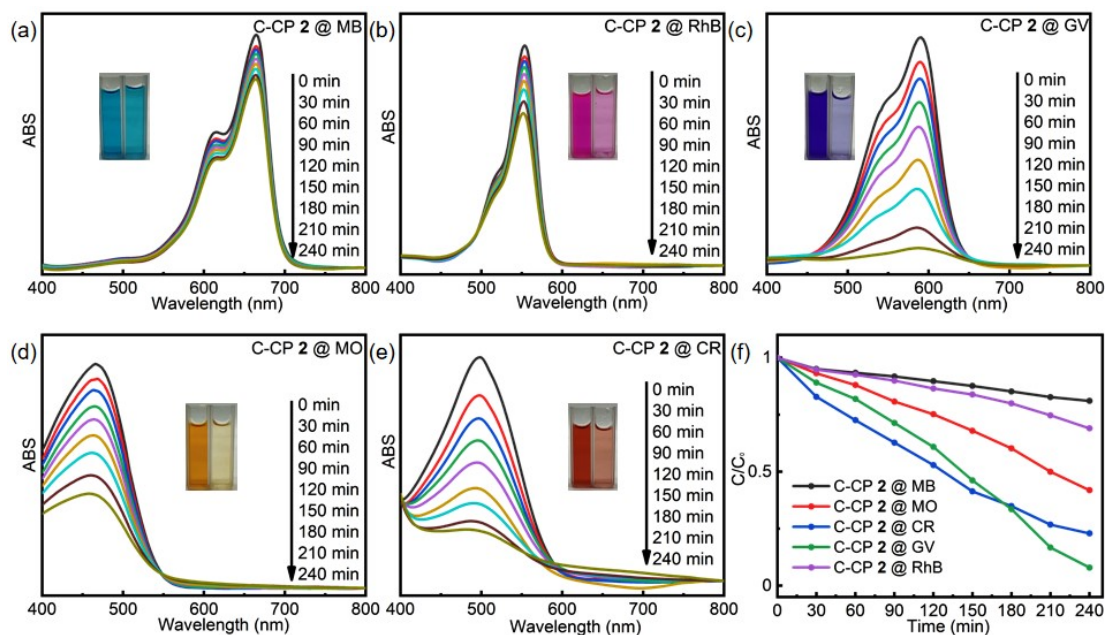

Fig. S3 UV–vis spectra of MB (a), RhB (b), GV (c), MO (d), and CR (e) solutions which were recorded after photocatalytic degradation had been performed for different lengths of time with C-CP **1**. (f) The photodegradation rates of MB, RhB, MO, CR and GV at different time points during exposure to C-CP **1**.
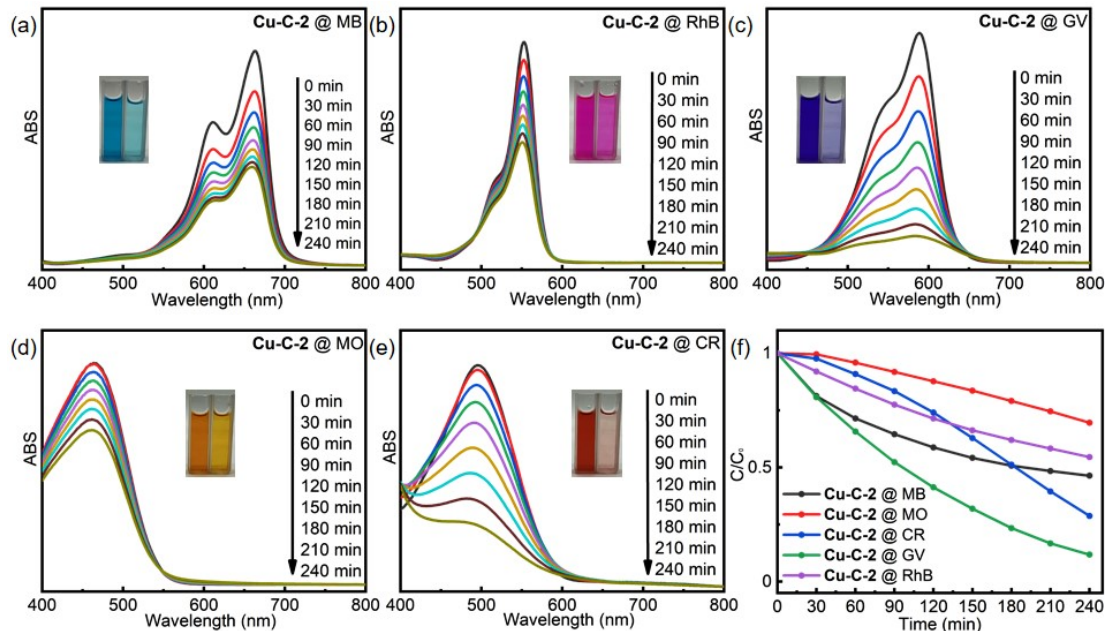
Fig. S4 UV–vis spectra of MB (a), RhB (b), GV (c), MO (d), and CR (e) solutions which were recorded after photocatalytic degradation had been performed for different lengths of time with C-CP **2**. (f) The photodegradation rates of MB, RhB, MO, CR and GV at different time points during exposure to C-CP **2**.
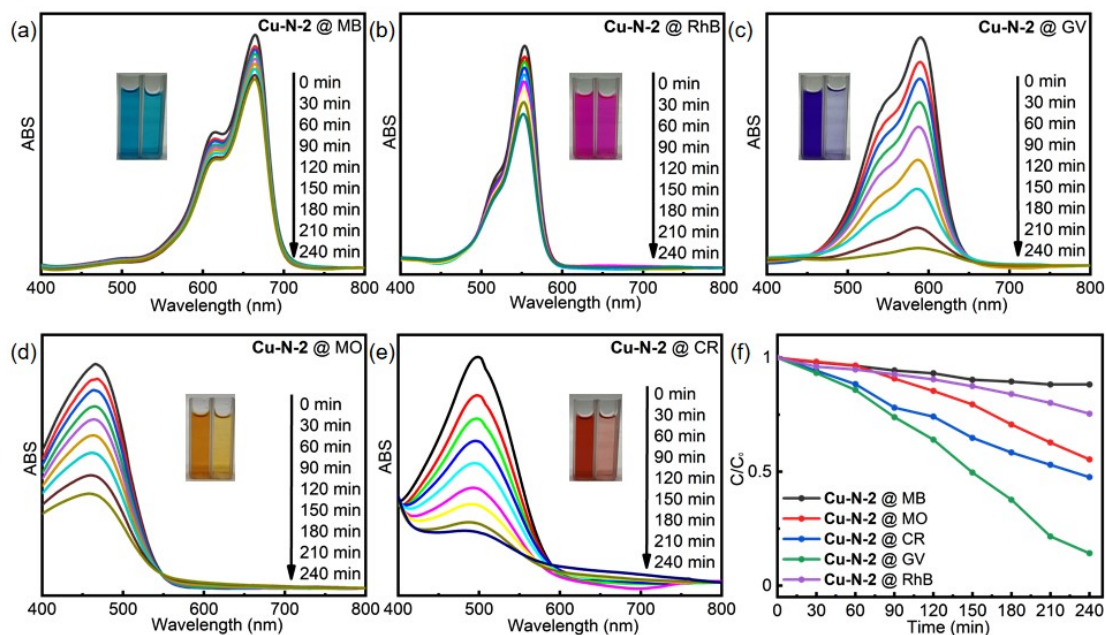

Fig. S5 UV–vis spectra of MB (a), RhB (b), GV (c), MO (d), and CR (e) solutions which were recorded after photocatalytic degradation had been performed for different lengths of time with **Cu-C-2**. (f) The photodegradation rates of MB, RhB, MO, CR and GV at different time points during exposure to **Cu-C-2**.

Fig. S6 UV–vis spectra of MB (a), RhB (b), GV (c), MO (d), and CR (e) solutions which were recorded after photocatalytic degradation had been performed for different lengths of time with **Cu-N-2**. (f) The photodegradation rates of MB, RhB, MO, CR and GV at different time points during exposure to **Cu-N-2**.
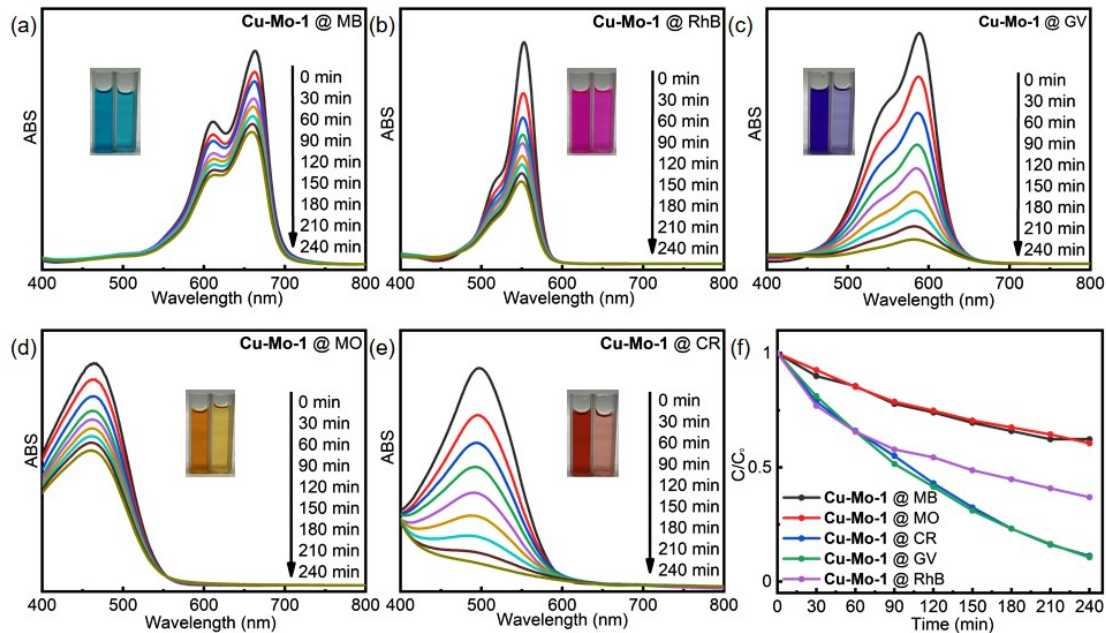

Fig. S7 UV–vis spectra of MB (a), RhB (b), GV (c), MO (d), and CR (e) solutions which were recorded after photocatalytic degradation had been performed for different lengths of time with **Cu-Mo-1**. (f) The photodegradation rates of MB, RhB, MO, CR and GV at different time points during exposure to **Cu-Mo-1**.
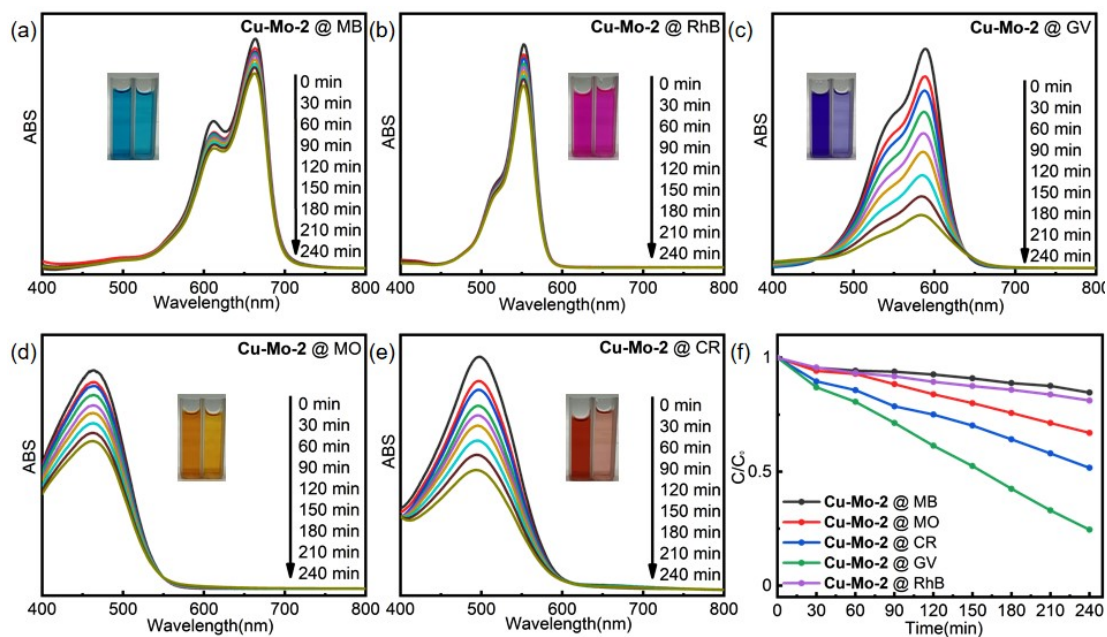
Supporting Information

Fig. S8 UV–vis spectra of MB (a), RhB (b), GV (c), MO (d), and CR (e) solutions which were recorded after photocatalytic degradation had been performed for different lengths of time with **Cu-Mo-2**. (f) The photodegradation rates of MB, RhB, MO, CR and GV at different time points during exposure to **Cu-Mo-2**.
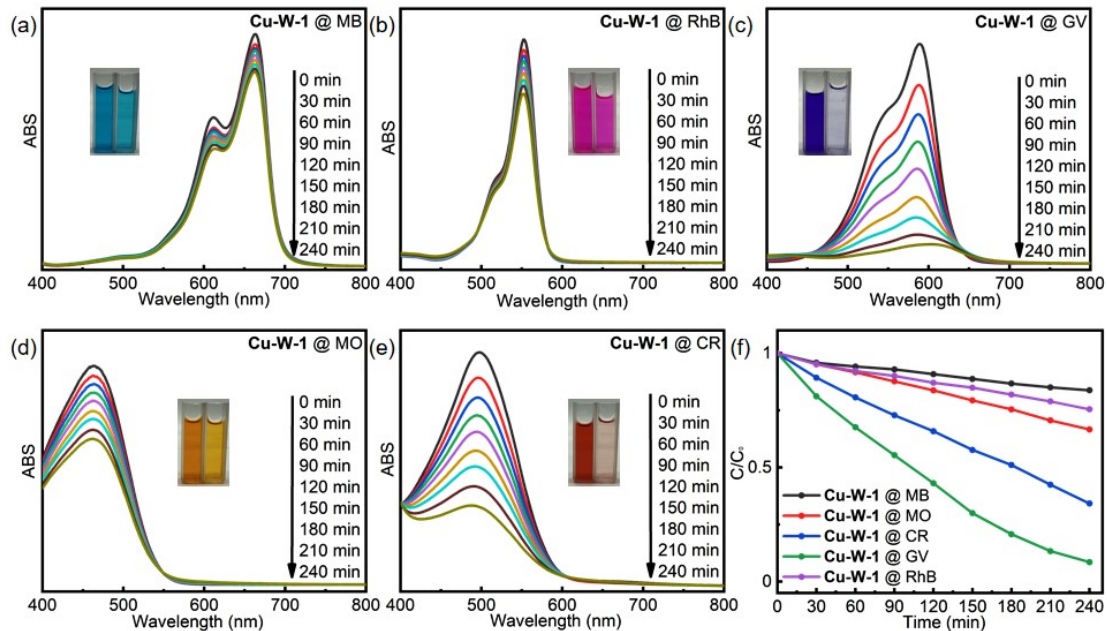

Fig. S9 UV–vis spectra of MB (a), RhB (b), GV (c), MO (d), and CR (e) solutions which were recorded after photocatalytic degradation had been performed for different lengths of time with **Cu-W-1**. (f) The photodegradation rates of MB, RhB, MO, CR and GV at different time points during exposure to **Cu-W-1**.
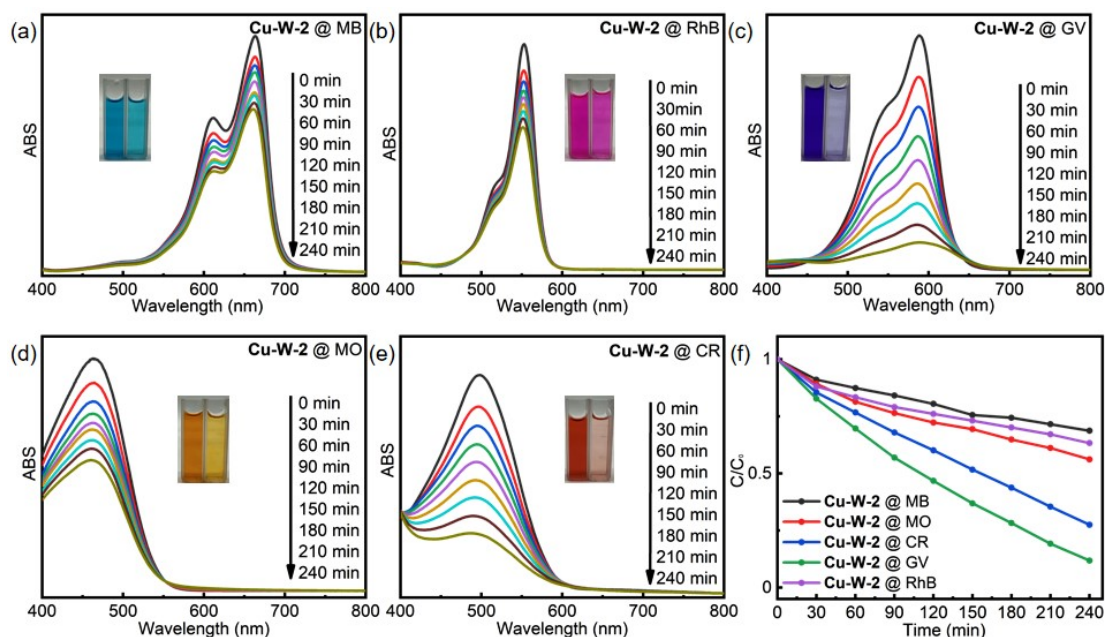
Fig. S10 UV–vis spectra of MB (a), RhB (b), GV (c), MO (d), and CR (e) solutions which were recorded after photocatalytic degradation had been performed for different lengths of time with **Cu-W-2**. (f) The photodegradation rates of MB, RhB, MO, CR and GV at different time points during exposure to **Cu-W-2**.
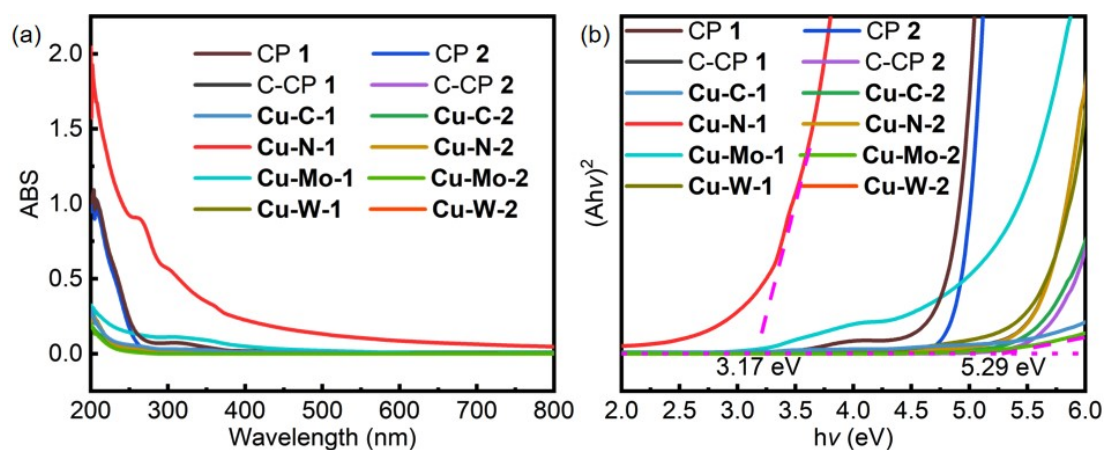

Fig. S11 (a) UV–vis absorption spectra of the Cu-CPs, CP-derived and CP-doping-derived structures; (b) Tauc's plots of the Cu-CPs, CP-derived and CP-doping-derived structures.

Supporting Information

S1. Pseudo-first-order kinetics.

These calculations were performed via equations (S1) and (S2):

$$\ln\left(C_0/C_t\right) = kt \qquad \text{(S1)}$$

$$t_{1/2} = \frac{ln2}{k} \qquad \text{(S2)}$$

where C_0 represents the initial concentration of dye (mg L^{-1}), C_t is the residual concentration of dye at time t (min), k denotes the pseudo-first-order rate constant (min^{-1}), and $t_{1/2}$(min) represents the half-life period of the reaction.

S2. Pseudo-second-order kinetics.
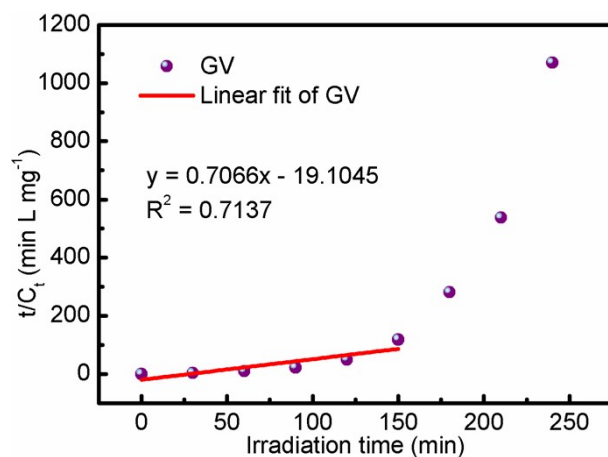
These calculations were performed via equations (S3):

$$t/C_t = 1/(kC_t^2) + t/C_0 \qquad \text{(S3)}$$

where C_0 represents the initial concentration of dye (mg L^{-1}), C_t is the residual concentration of dye at time t (min), and k denotes the pseudo-second-order rate constant (L mg^{-1} min^{-1}).

(a)
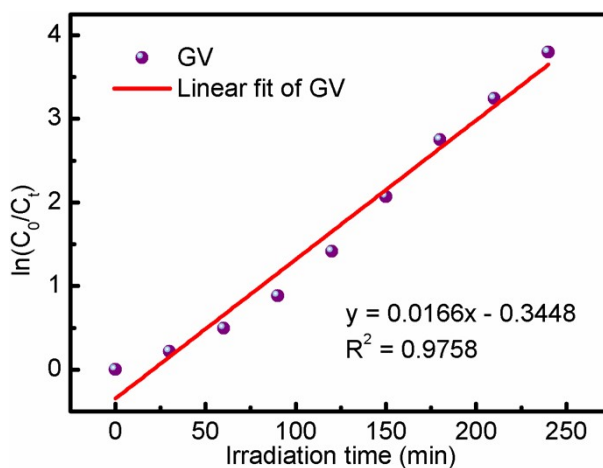
(b)

Fig. S12 (a) Pseudo-first-order plots with respect to time for **Cu-N-1** in GV solution; (b) Pseudo-second-order plots with respect to time for **Cu-N-1** in GV solution.
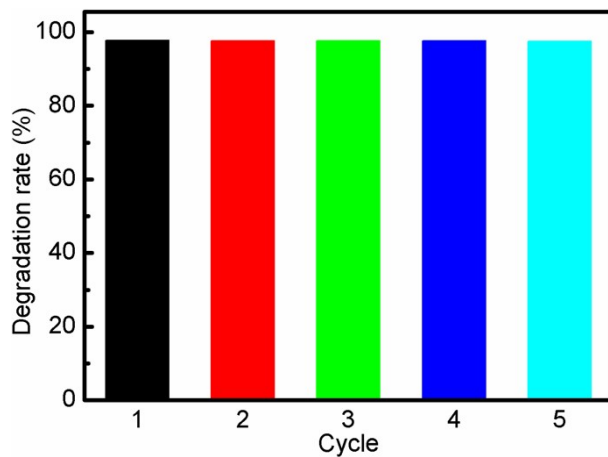

Fig. S13 The reproducibility of the photocatalyst **Cu-N-1** for GV.

Supporting Information

S3. Supplementary X-ray crystallography

First, the residual density plot of CP **2** has been shown in Fig. S14. The yellow balls of Q1–Q5 (residual peak <1) are revealed in ablow residual density plot. Second, the phenomenon of "over-assigned" Cu atom (Fig. S15) is a "crystallographic artifact", which is due to insufficient absorption correction. Thrid, we have measured the inductively coupled plasma spectrometer (ICP), X-ray photoelectron spectroscopy (XPS) and X-ray fluorescence (XRF) for CP **2** to verify the structural composition (Table S6). Moreover, the PXRD pattern for CP **2** was in agreement with the corresponding simulated one (Fig. 3d), indicating the phase purity of the sample and verifying the existence of Cu and the accuracy of SCXRD. Furthermore, there were only five elements such as Cu, C, N, O and H in the reactants, while there was nothing present at this site as well.
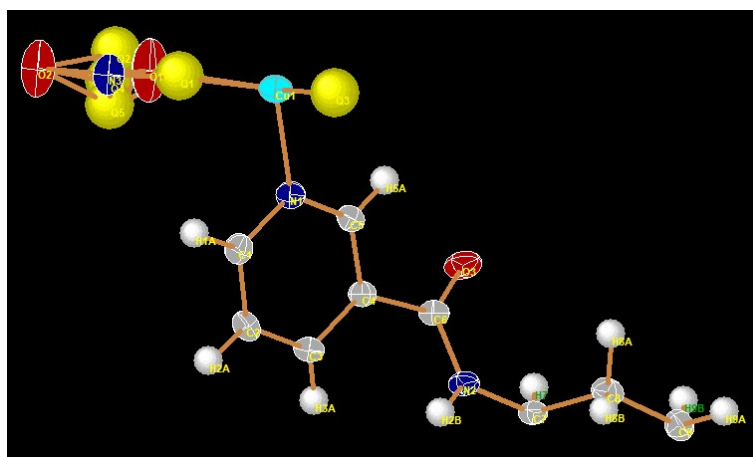

Fig. S14 The residual density plot of CP **2** (The yellow balls of Q1–Q5 (residual peak <1) are revealed in ablow residual density plot.).
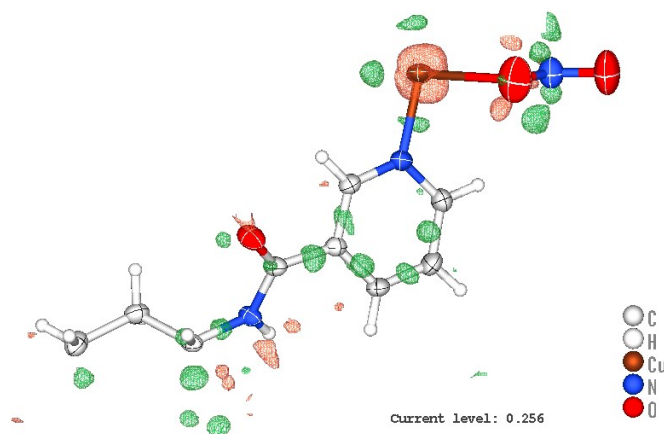

Fig. S15 The assigned density plot of CP **2**.

Supporting Information

Table S6 The elemental analysis and structural composition of CP **2**.

Element	ICP (%)	XPS (%)	XRF (%)	Theoretical value (%)
Cu	14.14	14.07	14.11	14.12
C	48.00	48.04	48.03	48.05
N	15.56	15.58	15.55	15.57
O	17.82	17.80	17.77	17.78